

RSC Advances



This is an *Accepted Manuscript*, which has been through the Royal Society of Chemistry peer review process and has been accepted for publication.

Accepted Manuscripts are published online shortly after acceptance, before technical editing, formatting and proof reading. Using this free service, authors can make their results available to the community, in citable form, before we publish the edited article. This *Accepted Manuscript* will be replaced by the edited, formatted and paginated article as soon as this is available.

You can find more information about *Accepted Manuscripts* in the [Information for Authors](#).

Please note that technical editing may introduce minor changes to the text and/or graphics, which may alter content. The journal's standard [Terms & Conditions](#) and the [Ethical guidelines](#) still apply. In no event shall the Royal Society of Chemistry be held responsible for any errors or omissions in this *Accepted Manuscript* or any consequences arising from the use of any information it contains.

Cite this: DOI: 10.1039/c0xx00000x

www.rsc.org/xxxxxx

ARTICLE TYPE

Conversion of Polystyrene into Porous Carbon Sheet and Hollow Carbon Shell over Different Magnesium Oxide Templates for Efficient Removal of Methylene Blue

Yanliang Wen^{a,b}, Jie Liu,^{*b} Jiangfeng Song,^{*a} Jiang Gong,^b Hao Chen^b and Tao Tang^{*b}*Received (in XXX, XXX) Xth XXXXXXXXX 20XX, Accepted Xth XXXXXXXXX 20XX*

DOI: 10.1039/b000000x

Abstract: Conversion of waste polymer on metal-free catalyst is a promising method for the preparation of nanocarbon. Herein, we synthesized porous carbon sheet and hollow carbon shell through the carbonization of polystyrene on magnesium oxide with different morphologies at 700 °C using a one-pot method. The morphologies, microstructure, phase structure, surface element composition, thermal stability, and textural properties of the obtained nanocarbon were analyzed by SEM, TEM, XRD, TGA, and Raman. The yield of nanocarbon increased as the weight ratio of magnesium oxide to polystyrene increased. Magnesium oxide acted as a template for the shape-controlled growth of carbon nanostructure. The surface area of porous carbon sheet and hollow carbon shell reached 854 and 523 m²/g without any activation, respectively. The porous carbon sheets were used as adsorbents to remove methylene blue from water and showed an adsorption capacity of 358.8 mg/g. Product composition for the pyrolysis of polystyrene in the presence of magnesium oxide was analyzed using GC and GC-MS to elucidate the reaction mechanism. The yield of styrene in the liquid products reached 50% by the catalysis of polygonal magnesium oxide. This strategy provides a cheap and sustainable catalyst for converting polymer into high-value nanocarbon and useful chemicals.

Introduction

Upcycling of waste polymers into valuable carbon nanomaterials has attracted more attention owing to drastic increase in plastic waste. Nanocarbon have been prepared by decomposition of different polymers such as polyethylene (PE),¹ polypropylene (PP),² polystyrene (PS),³ polyvinyl chloride (PVC),⁴ and polyethylene terephthalate (PET)⁵ due to carbon is the major constituent of these polymers, thus these polymer wastes provide a carbon source for the production of nanocarbon. In addition, PP, PE, PS, PET, and PVC are the main components in household wastes. The produced nanocarbon include carbon nanotubes,⁶ carbon sphere,⁷ multi-layered graphene,⁸ and metal/carbon composites⁹. Typical methods of producing nanocarbon using plastics as carbon feedstock have been reviewed in the literature and can be classified into two categories: one-pot conversion and stepwise conversion.^{10,11}

In one-pot conversion, polymer degradation and the growth of carbon proceed simultaneously. The type and composition of polymer, reaction temperature, reactor type, and catalysts are the important factors affecting the yield and morphology of the obtained nanocarbon. Kong et al. synthesized straight and helical carbon nanotube and Fe₃O₄@C composite through catalytic decomposition of PE in an autoclave.¹² Pol et al. converted waste PE into carbon nanotube and carbon spheres using an autoclave

as a reactor under high pressure, which show high performances in lithium electrochemical cells.¹³ Our group found that the combination of solid acid with nickel based catalyst is efficient for high-yield conversion of plastics into carbon nanotube under atmospheric pressure.¹⁴ Solid acid promote the degradation of polymer into light hydrocarbons and aromatics and then the resultant organic compounds react on the surface of nickel based catalyst.¹⁵

Although nanocarbon with a diversity of morphologies have been synthesized from different polymers using combined catalysts, the high cost of transition metal prompted us to explore a new facile method to convert waste polymers to nanocarbon. Recently, we synthesized graphene flakes consisting of several to a dozen layers of graphene layers by catalytic carbonization of waste PP using organically modified montmorillonite as degradation catalyst and template at 700 °C.¹⁶ This approach provides a novel way to prepare graphene flakes on the metal-free catalyst using waste plastics as carbon sources. However, the purification of the obtained char involves removal of montmorillonite by hydrofluoric acid, which is dangerous, tedious and time consuming. The morphology of the nanocarbon also needs to be improved. The surface area of the obtained nanosheet is low and requires additional activation in potassium hydroxide at 700 °C to increase, which further increased the cost of the technology.

Magnesium oxide (MgO) is a basic alkali earth oxide and can be easily removed by diluted acid. MgO can also be used as a catalyst for the growth of nanocarbon by chemical vapor deposition.¹⁷ Porous graphene,¹⁸ few-layer graphene shells,¹⁹ and nitrogen-doped amorphous graphene²⁰ have been synthesized on MgO substrate by chemical vapor deposition. However, no studies have investigated the conversion of polymer into nanocarbon on MgO substrate.

Herein, we synthesized nanocarbon using PS as carbon source on MgO at 700 °C. The effects of the type and the amount of MgO on the yield, morphology, structure, and textural properties of the obtained nanocarbons were studied. The product composition for pyrolysis of PS in the presence of MgO was analyzed using GC and GC-MS. The potential application of produced nanocarbons in adsorption of MB was also explored.

Experimental

Materials

Polystyrene (PS, trademark PG-383) pellets were provided by Zhenjiang Qimei Chemical Co., Ltd., China. The sheet MgO was purchased from Xilong Chemical Co., Ltd., China. The polygonal MgO was supplied by Tianjin Fuchen Chemical Reagents Factory. All chemicals were of analytical-grade quality.

Preparation of nanocarbons

MgO and PS were mixed in a crucible and then heated at 700 °C for 6 min in a self-prepared carbonization equipment, which has been described in a previous report.⁹ Each crucible was covered by crucible lid. After carbonization, the resultant residue was purified using 18 wt% hydrochloric acid solution to eliminate MgO. Subsequently, the samples were washed using deionized water and ethanol and finally dried at 80 °C for 24h under vacuum. The isolated porous carbon sheet and hollow carbon shell were denoted as PCS-*x* and HCS-*x*, respectively, where *x* represented the weight ratio of MgO to PS. The yield of PCS-*x* and HCS-*x* was calculated by dividing the amount of purified carbon product by the amount of PS. Each measurement was repeated three times for the reproducibility purpose.

Pyrolysis experiment

Pyrolysis of PS and PS/MgO were conducted at 700 °C in a fixed bed reactor. The quartz tube was horizontally mounted in an electrical resistance furnace and heated to 700 °C in N₂ atmosphere (N₂ was used to blow off the air in the tube before pyrolysis and the degraded products after pyrolysis). Subsequently, the desired sample was put into the quartz tube and pyrolyzed at 700 °C. The liquid pyrolyzed products were collected using a cold trap in ice water and the gaseous products were collected using a sample bag.

Characterization

The morphologies of nanocarbons were characterized on a field-emission scanning electron microscopy (FE-SEM, XL30ESEM-FEG) and a transition electron microscopy (TEM, JEM-1011, an accelerating voltage of 100 kV). The microstructure of nanocarbons was observed by high-resolution transition electron microscopy (HRTEM) on a FEI Tecnai G2 S-Twin transmission electron microscope operating at 200 kV. Thermal stability of the

nanocarbon were measured by thermal gravimetric analysis (TGA) under air flow (100 mL/min) from room temperature to 800 °C at a heating rate of 10 °C/min on a TA Instruments SDT Q600. The phase structure of obtained nanocarbon was analyzed by X-ray diffraction (XRD) using a D8 advance X-ray diffractometer with Cu K α radiation operating at 40 kV and 200 mA. Raman spectroscopy (T6400, excitation beam wavelength = 514.5 nm) was used to characterize the vibrational properties of obtained nanocarbon. The surface element composition of obtained nanocarbon were characterized by means of X-ray photoelectron spectroscopy (XPS) carried out on a VG ESCALAB MK II spectrometer using an Al K α exciting radiation from an X-ray source operated at 10 kV and 10 mA. The textural properties of obtained nanocarbon were measured by nitrogen adsorption/desorption at 77 K using a Quantachrome Autosorb-1C-MS analyzer. The specific surface area was calculated by the Brunauer–Emmett–Teller (BET) method. The liquid fraction of pyrolyzed products from PS at 700°C were weighed and then analyzed by gas chromatography–mass spectrometry (GC–MS, AGILENT 5975MSD). Gas products were collected at room temperature under atmospheric pressure. The volume of collected gas products was determined by the displacement of water. The organic gas products (C1–C4) were analyzed by a GC (Kechuang, GC 9800) equipped with a FID, using a KB-Al₂O₃/Na₂SO₄ column (50 m×0.53 mm ID). H₂, N₂, and CH₄ were analyzed by a GC (Kechuang, GC 9800) equipped with a TCD, using a packed TDX-01 (1 m) and a molecular sieve 5A column (1.5 m).

Adsorption experiment

Adsorption experiment of MB by PCS-10 and HCS-10 was carried out in a batch process by stirring 0.025 g of nanocarbon in 50 mL of MB solution in a 100 mL polyethylene flask at 20 ± 1 °C. Solution of adsorbate was prepared from the stock solution (1000 mg/L) to the desired concentration for each experimental run. The 0.5 mol/L HCl solution was used to adjust the pH of MB solution to be stable at about 6. After stirring for 240 min, 1 mL of MB solution was withdrawn by a syringe and then was diluted and filtered through 0.25 μm membrane for later analysis of MB concentration. The concentration of MB solution was measured by UV/Vis/NIR spectrophotometer (Lambda 900) to monitor the absorbance at $\lambda_{\text{max}} = 665 \pm 1$ nm, corresponding to the maximum absorbance. The concentration of MB solution was determined by linear regression equation, which was obtained by plotting the calibration curve for MB over a range of concentrations.

Results and discussion

Yields of PCS and HCS

Fig. 1 displays the effect of weight ratio of MgO to PS on the yield of nanocarbon obtained on sheet and polygonal MgO through catalytic carbonization of PS at 700 °C. Magnesium oxide was roasted in muffle furnace at 700 °C for 2 h and then kept in drying apparatus to eliminate the variation of the mass. Sheet MgO exhibited a little higher yield of carbon than that over polygonal MgO, which may be attributed to the higher surface area of sheet MgO (47 m²/g, and that of polygonal MgO was 13 m²/g). In addition, the yield of PCS and HCS increased when the weight ratio of MgO to PS increased. For example, when MgO/PS weight ratio was increased from 1 to 10, the yield of

PCS increased from 6 to 16 wt%, indicating that the amount of MgO promote the production of nanocarbon. When the weight ratio of polygonal MgO/PS increased, the yield of HCS increased and reached a maximum of 10.8 wt% at a weight ratio of MgO/PS of 7.5. Temperature is another core component that affects the growth of nanocarbon. Only 0.3 and 1 wt% of carbon was produced on sheet MgO at 500 and 600 °C (Table S1), respectively.

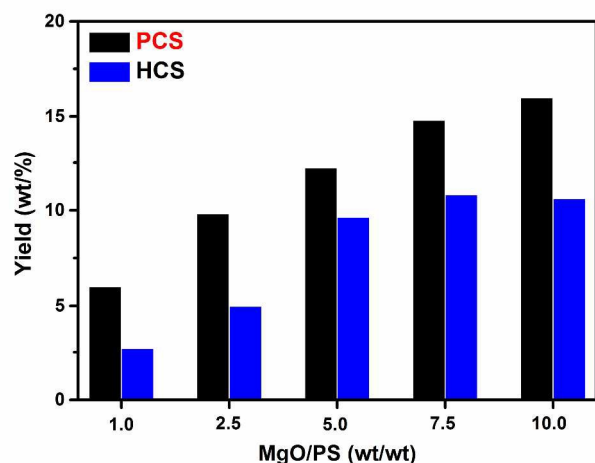


Fig. 1 Effect of the weight ratio of MgO to PS on the yield of nanocarbon through catalytic carbonization of PS at 700 °C.

Morphology and microstructure of MgO and synthesized nanocarbon

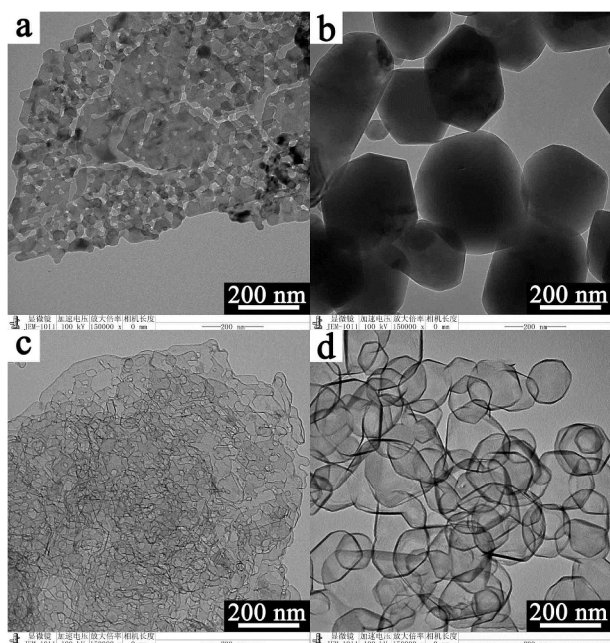


Fig. 2 TEM images of (a) sheet MgO, (b) polygonal MgO, (c) PCS-10 and (d) HCS-10.

Fig. 2 shows the TEM images of MgO and obtained nanocarbon. Two types of MgO were sheet and polygonal, respectively. The diameter of polygonal MgO ranged from dozens of nanometers to hundreds of nanometers. PCS-10 was sheet carbon (Fig. 2c) and HCS-10 (Fig. 2d) was hollow carbon shell resembling the initial morphology of MgO, which indicate that MgO act as a template

for the shape-controlled growth of carbon nanostructures. Many mesopores were found on the carbon sheet (Fig. 2c). No impurities such as amorphous carbon were found. The obtained carbon on sheet MgO at 500 and 600 °C was amorphous (Fig. S1). At 800 °C, the morphology of the carbon resembled to that of the carbon obtained at 700 °C.

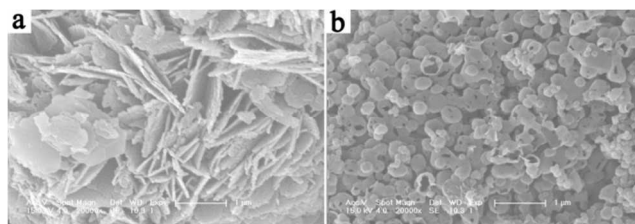


Fig. 3 SEM images of (a) PCS-10 and (b) HCS-10.

Fig. 3 shows the SEM images of the nanocarbon. In Fig. 3a, PCS stacked together, which may be due to that the carbon deposited on the both sides of sheet MgO. When sheet MgO was removed, space between two graphene layers appeared. Hollow carbon shell was obtained on polygonal MgO (Fig. 3b). However, most of carbon shells were broken, which may be due to that part of polygonal MgO agglomerated during carbonization, leading to that hydrocarbons could not fully contact with polygonal MgO.

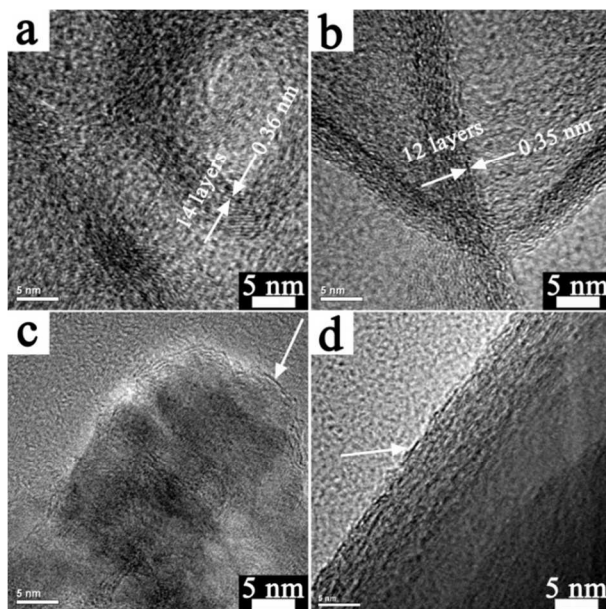


Fig. 4 HRTEM micrographs for (a) PCS-10, (b) HCS-10, (c) sheet MgO@PCS-10 and (d) polygonal MgO@HCS-10.

Fig. 4 presents HRTEM images of PCS-10, HCS-10, sheet MgO@PCS-10 and polygonal MgO@HCS-10. Stacked graphene layer coated on the surface of MgO. The number of graphene layers ranged from 12 to 16 for both samples, indicating the formation of graphite nanosheet.

Based on the above results, it could be demonstrated that both sheet MgO and polygonal MgO acted as the template for the growth of graphite nanosheet during the carbonization of PS.

Phase structure, surface element composition, thermal stability, and textural properties of the produced nanocarbons

Fig. 5 shows the XRD patterns of MgO, MgO@C, and isolated nanocarbons. The diffraction peaks at $2\theta = 36.9^\circ$ (111), 42.9° (200), 62.3° (220), 74.6° (311), and 78.6° (222) were attributed to the MgO phase. No difference was found between the two templates. MgO phase in the MgO@C after carbonization reaction indicates the unchanged structure of MgO. When MgO was removed, the diffraction peaks of MgO disappeared completely and two weak and broad diffraction peaks at $2\theta = 26.2^\circ$ and 43.0° appeared. These two peaks were assigned to the typical graphitic (002) and (101) planes, respectively. The broad peak of the nanocarbon reflected the disorder and irregular arrangement of carbon layers, which agreed well with HRTEM observation.

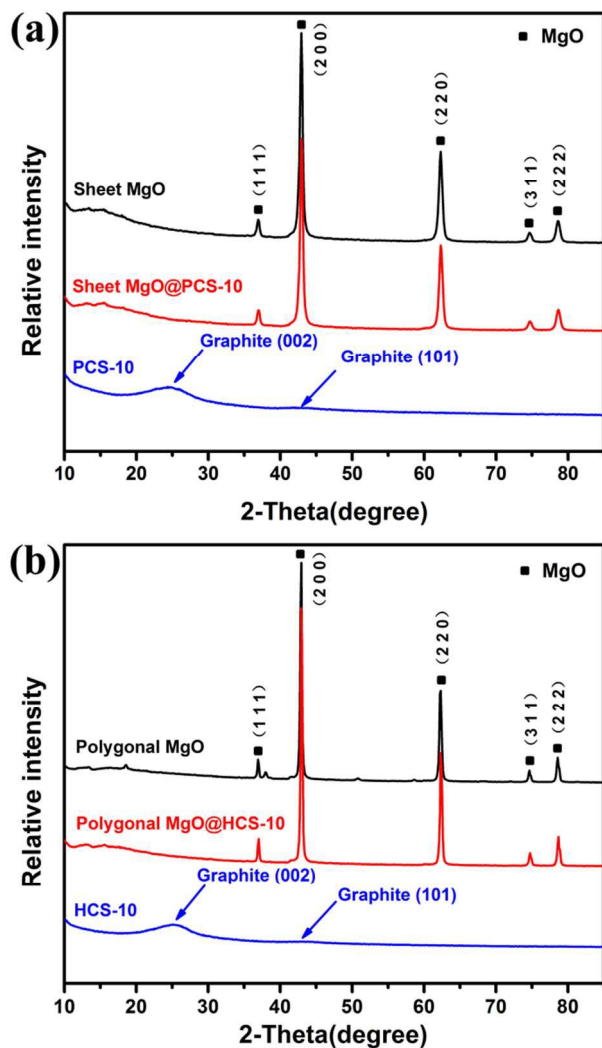


Fig. 5 XRD patterns of MgO, MgO@C and isolated nanocarbon.

Raman spectroscopy was used to identify the presence of sp^2 carbon. Fig. 6 presents Raman spectra of PCS-10, PCS-1, HCS-10, and HCS-1. All the spectra show typical spectral characteristics of graphitic carbon: the D-band ($\sim 1350\text{ cm}^{-1}$) and the G-band ($\sim 1580\text{ cm}^{-1}$). The D-band is associated with vibration of carbon atoms with dangling bonds in the plane terminations of disordered graphite or glassy carbons, indicating the structural defects and partially disordered structures of sp^2 carbon. The G-band corresponds to the first-order scattering of an E_{2g} vibrational

mode of hexagonal graphite and is related to the vibration of sp^2 -bonded carbon atoms in a graphite layer, which can be used to explain the degree of graphitization.^{21,22} The intensity ratio of I_G/I_D for the four samples was about 0.9, which suggests the obtained nanocarbons are defective. This result may be due to the vacancies or the edges on the graphene layer. The weight of MgO to PS had little effect on the graphitization of the nanocarbons. The degree of graphitization of the porous carbon sheet was increased by increasing reaction temperature (Fig. S2). The order of the carbon can also be improved by post-heat treatment of the carbon products at high temperatures ($>2000\text{ }^\circ\text{C}$) in an inert atmosphere. In addition, incorporation of Fe, Co, and Ni based catalysts in MgO may increase the degree of graphitization. These ideas will be attempted in the following experiment to increase the graphitization of the carbon.

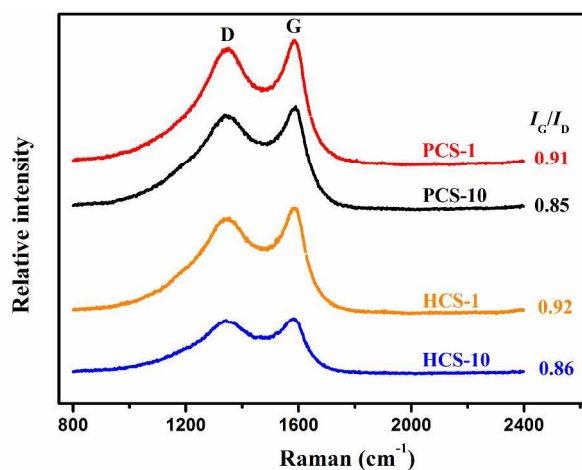


Fig. 6 Raman spectra of PCS and HCS.

Fig. 7a shows the XPS spectra of PCS-10 and HCS-10. The composition of carbon and oxygen for both two samples was about 97% and 3%, respectively. C1s (284.8 eV) and O1s (532.6 eV) peaks in the survey scan spectra indicated that MgO is completely removed. The XPS spectra of C1s were curve-fitted into three individual peaks (Fig. 7b and 7c) to determine the chemical component and oxidation state of carbon: graphitic carbon (284.8 eV), C–OH (285.5–285.7 eV), and C=O (286.8–287.1 eV).²³ Compared with the HCS, the PCS possessed relatively less graphite carbon and more C=O groups. The functional groups containing oxygen could contribute to remove heavy metallic ions^{24,25} or organic dyes²⁶ when PCS or HCS were used as adsorbents in wastewater treatment.

Fig. 8 shows the TGA and DTG curves of PCS-10 and HCS-10 under air. The weight loss of PCS and HCS exhibited two stages. The weight loss from 100 to $300\text{ }^\circ\text{C}$ was attributed to the release of chemisorbed water and the pyrolysis of oxygen containing functional groups on the surface of the resultant carbon materials.²⁷ From 400 to $700\text{ }^\circ\text{C}$, a remarkable weight loss was ascribed to the oxidation of the carbon.²⁸ The maximum oxidation temperatures of the two samples were centered at about $630\text{ }^\circ\text{C}$. The residues of them at $800\text{ }^\circ\text{C}$ were calculated to be less than 2 wt%, indicating the high purities of both PCS and HCS.

Nitrogen adsorption/desorption experiments were carried out at 77 K to characterize the textural properties of PCS and HCS. The BET surface area (S_{BET}), mesopore surface area (S_{meso}), total pore volume (V_{total}), mesopore volume (V_{meso}), and average pore

diameter (D_{AV}) of PCS-10, PCS-1, HCS-10, and HCS-1 are summarized in Table 1. Although the surface area of sheet MgO was only 47 m²/g, the surface area of the produced carbon nanomaterial obtained on sheet MgO reached 854 m²/g. The weight ratio of PS to MgO had no effect on the specific surface area and average diameter of the pores for both PCS and HCS. The surface area of PCS-10 (854 m²/g) was far higher than that of HCS-10 (523 m²/g), which can be attributed to the higher surface

area of sheet MgO (47 m²/g, and that of polygonal MgO was 13 m²/g). All the samples exhibited a hysteresis loop (Fig. 9a), which are characteristics of mesopores. The pore size distributions of PCS and HCS were calculated using the Barrett–Joyner–Halenda (BJH) model from the desorption branches of the isotherms (Fig. 9b). Interestingly, no matter what types of MgO or weight ratio of PS to MgO was used, the diameter of mesopores located in a narrow range of 2 to 6 nm (centered at about 3.8 nm). From the above results, we can conclude that the textural properties of the produced nanocarbons are independent of the volume and diameter of pores on MgO. The porosity may come from the assembling of the reactant.

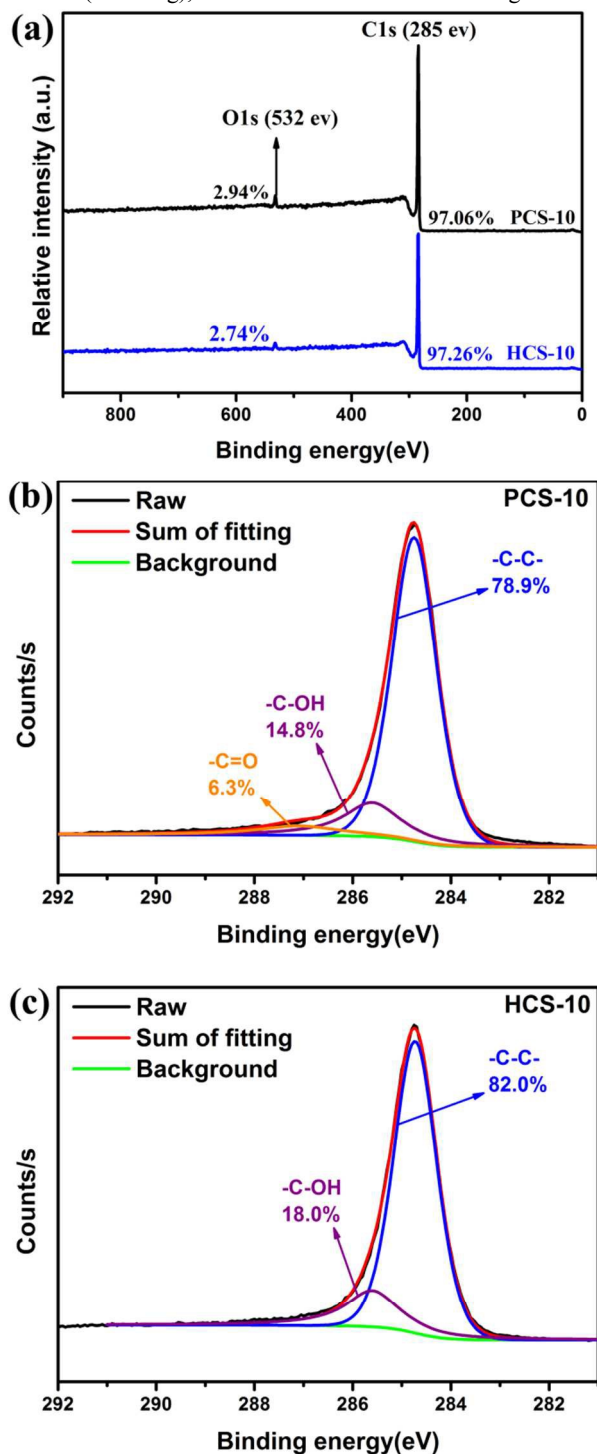


Fig. 7 XPS spectra of the PCS-10 and HCS-10 (a), and deconvoluted C1s spectra of PCS-10 (b) and HCS-10 (c).

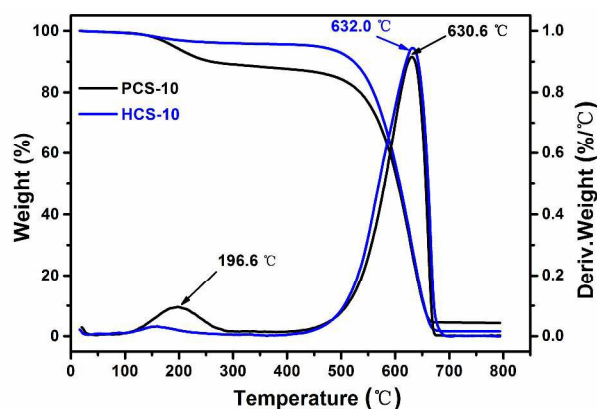


Fig. 8 TGA and DTG curves of PCS-10 and HCS-10 under air.

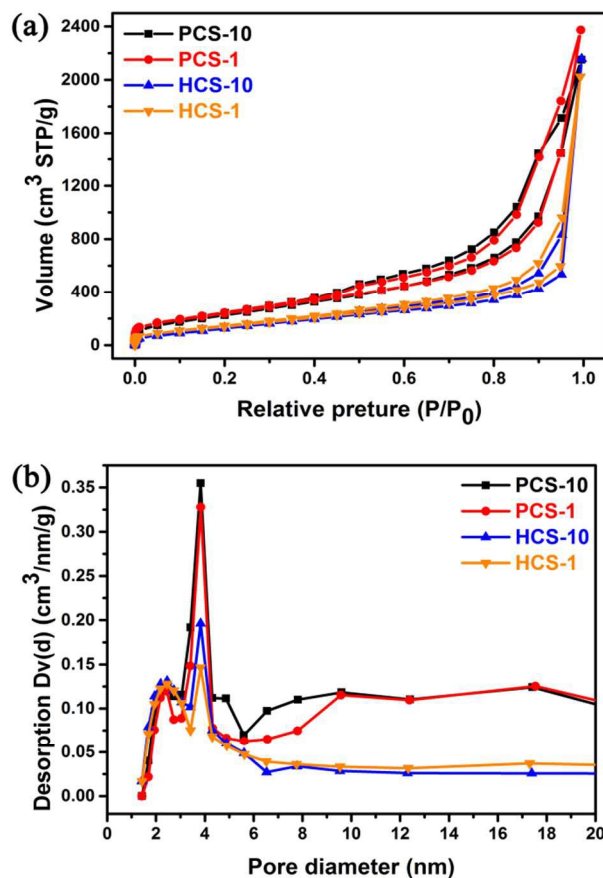


Fig. 9 Nitrogen adsorption/desorption isotherms (a) and pore size distributions (b) of PCS and HCS.

Table 1 Textural properties of MgO and obtained nanocarbons.

Properties	S_{BET} (m ² /g) ^a	S_{meso} (m ² /g) ^b	V_{total} (cm ³ /g) ^c	V_{meso} (cm ³ /g) ^d	D_{AV} (nm) ^e
Sheet MgO	47	47	0.341	0.341	47.7
Polygonal MgO	13	10	0.062	0.058	33.3
PCS-10	854	854	3.326	3.326	3.8
PCS-1	854	854	3.672	3.672	3.8
HCS-10	523	523	3.337	3.337	3.8
HCS-1	537	537	3.131	3.131	3.8

^a The total specific surface area.^b The specific surface area of mesopores.^c The total volume.^d The volume of mesopores.^e The average diameter of pores.

Effect of the types of MgO (sheet or polygonal) on the mass balance, composition of liquid and gaseous products

The degraded products of PS are the precursors to form carbon. Composition of the degraded products was analyzed by GC and GC-MS to study the reaction mechanism. Table 2 shows the yields of different fractions and composition of the gases for the pyrolysis of PS and PS/MgO with two different ways of mix. Pyrolysis of PS produced 99.5 wt% of liquid oil and 0.2 wt% of gas at 700 °C. When the thermally degraded products of PS passed through sheet MgO, only 0.6 wt% of carbon was produced. When PS and sheet MgO was mixed and heated, about 12.2 wt% of carbon was produced. These results indicate that the degraded products of PS catalyzed by MgO are effective as feedstock to the growth of carbon. PS produced 99.5 wt% of liquid and PS/sheet MgO produced 87.1 wt% liquid. The yield of gases varied little for all samples. These results indicate that liquid products are the main feedstock for the growth of carbon. In conclusion, MgO not only acted as a template for growth of nanocarbon but also functioned as a degradation catalyst, which affected the composition of the liquid products of PS.

Table 2 also displays the composition of the gas from pyrolysis of PS and PS/MgO. The gaseous products mainly consisted of hydrogen, methane, ethane, ethylene, propane, propylene, *i*-butene, and pentene. When PS was pyrolyzed and passed through MgO, the yields of ethylene and C₃-C₅ gases decreased, whereas the yield of hydrogen and methane increased. MgO promote the conversion of C₂-C₅ gases into hydrogen and methane. Nevertheless, when MgO and PS were decomposed via one-pot method, the yield of hydrogen further increased, whereas the yield of methane decreased, implying that MgO could catalyze the decomposition of methane into carbon and hydrogen.

Fig. 10 shows the GC profiles for the liquid fraction of pyrolyzed products from PS and PS/MgO (sheet and polygonal). The assignment and the area percentages of the peaks are given in Table S2. These components were grouped into different classes by the number of benzene rings (Table 3). The area percentages of three main peaks are also shown in Table 3. 2,4-diphenyl-1-butene and 2-phenyl-1,2,3,4-tetrahydronaphthalene are dimmers of styrene. Styrene and its dimers were identified as major products in the liquid. When the degradation products of PS passed through MgO (two-stage), the yield of dimers of styrene

decreased, whereas the yield of styrene increased. Considering there was almost no carbon produced, we can conclude that the compounds with two benzene rings cracked into compounds with one benzene ring (including styrene). The compounds with one or two benzene rings were not the carbon source for the growth of nanocarbons. The one-pot method can be considered as a combination of MgO catalyzed degradation of PS and carbonization of degradation products on MgO. The yield of styrene from both one-pot and two-stage process was close. The yield of dimers of styrene decreased, whereas the yield of compounds with three benzene rings increased. These results indicate that MgO promote the degradation of PS into aromatics with three benzene rings or more, which are the main carbon source for the growth of nanocarbon. The increasing trend is more evident on sheet MgO and more carbon is produced at the same time, which verifies the above conclusion.

A possible mechanism was proposed to explain the formation of porous carbon sheet and hollow carbon shell through catalytic carbonization of PS by MgO based on the above results. Degradation of PS began with chain scission promoted by heat and basic sites on MgO. From GC-MS results, the compounds with three benzene rings or more were the main carbon source for the growth of nanocarbon on MgO. Styrene and its dimers were identified as major products in the liquid. Polycyclic aromatic hydrocarbons may be generated from styrene via hydrogen abstraction acetylene addition.²⁹ The traditional vapor-liquid-solid mechanism is not suitable for this case because carbon dissolution in MgO is impossible. The reaction probably proceeds through a bottom-up mechanism.³⁰ The polycyclic aromatic hydrocarbons absorbed and assembled on the surface of MgO to form graphene layer. Further carbon deposition led to the stacked graphene layer and thicker shell. Reilly et.al considered that carbon coating on the catalyst can decompose hydrocarbons but not poison catalyst.³¹ Thus, this is the reason why many pores existed on the obtained nanocarbon. The shape of the obtained nanocarbon is dependent on the initial morphology of MgO, which verifies the template-shaped role of MgO.

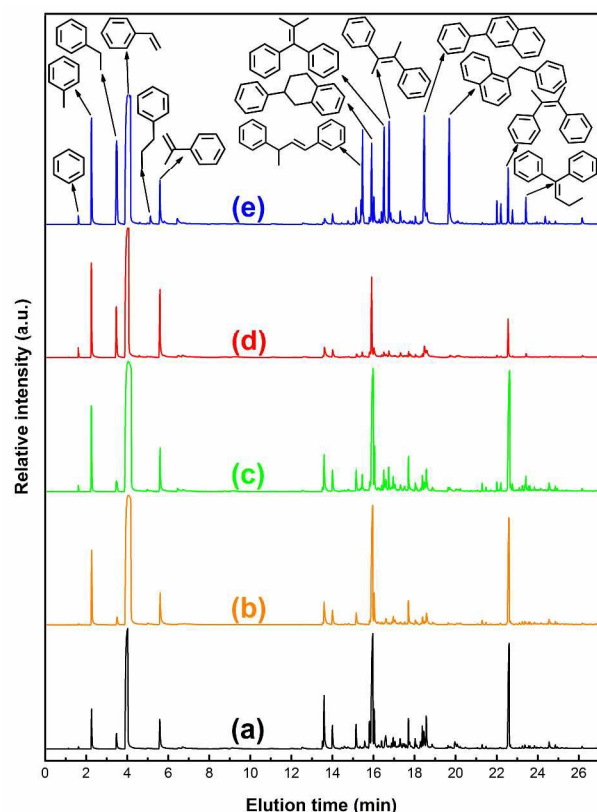


Fig. 10 GC-MS profiles of liquid decomposition products from PS and PS/MgO mixtures. (a) PS; (b) PS and polygonal MgO, separately; (c) PS and sheet MgO, separately; (d) PS/polygonal MgO mixture; (e) PS/sheet MgO mixture.

Adsorption of MB

PS were carbonized into PCS and HCS with a high surface area and large pore volume as well as abundant surface functional groups, which are useful in adsorption, using a facile and sustainable approach. As an example, PCS-10 and HCS-10 were chosen as model adsorbents for adsorption of MB from wastewater to explore the potential application of the resultant carbon materials.

The equilibrium isotherm was introduced to clarify the interaction between adsorbent and adsorbate. The correlation of the experimental results to the adsorption model helps to understand the adsorption mechanism. The Langmuir model was employed to analyze the experimental data for MB adsorption, which is represented by the following equation:

$$q_e = q_m \cdot K_L C_e / (1 + K_L C_e) \quad (1)$$

Where q_e (mg/g) is the interrelation of equilibrium adsorption capacity of MB on the PCS-10 or HCS-10, C_e (mg/L) is its equilibrium solute concentration, K_L is the Langmuir constant (L/mg) and q_m is the maximum adsorption capacity (mg/g), which depends on the number of adsorption sites. The amount of adsorbate taken up by adsorbent at the equilibrium time was calculated by the following expression:

$$q_e = (C_0 - C_e) / W \quad (2)$$

Where q_e (mg/g) and C_e (mg/L) are equal to the ones above, C_0 is the initial concentration of adsorbate in solution (mg/L), V (L) is the volume of solution and W (g) is the weight of adsorbent.

Table 2 Yields of the different fractions and gas compositions for the pyrolysis of PS and PS/MgO in two different ways of mix.

	PS	PS-Sheet MgO two-stage ^a	PS-Polygonal MgO two-stage ^a	PS-Sheet MgO one-pot ^b	PS-Polygonal MgO one-pot ^b
Carbon (wt%)	0.0	0.5	0.4	12.2	9.2
Liquid (wt%)	99.5	97.9	98.0	87.1	90.2
Gas (wt%) ^c	0.2	0.3	0.3	0.4	0.4
Gas (L/100g PS) ^d	0.3	0.6	0.4	1.3	1.1
Gas composition (vol%) ^e					
H ₂	36.7	63.5	45.3	89.1	75.8
CH ₄	17.5	21.6	22.9	7.2	12.7
C ₂ H ₄	39.2	12.1	25.0	2.7	9.5
C ₃ -C ₅	6.6	2.8	6.9	1.1	2.0

^a 5g of PS and 25g of MgO, separately.

^b Mixture of 5g of PS and 25g of MgO.

^c Calculated by the volume of the gas first divided by 22.4 L/mol, then multiply the volume percentage and the molar mass of different gases and finally add them together.

^d Calculated by the displacement of water.

^e Calculated by the volume of the gas divided by the total volume of gas products.

Table 3 The area percentage of the different classes of compounds and three main compounds in Fig. 10 that were produced by degradation of PS and the mixture of PS/MgO at 700 °C.

Substance	PS	PS-Sheet MgO two-stage ^a	PS-Polygonal MgO two-stage ^a	PS-Sheet MgO one-pot ^b	PS-Polygonal MgO one-pot ^b
Styrene,	27.2	42.6	51.1	36.2	50.2
(Z)-2,4-diphenyl-1-butene,	12.3	11.5	9.5	2.3	3.3
2-phenyl-1,2,3,4-tetrahydronaphthalene,	15.9	12.6	13.5	3.7	7.5
Classes of compounds (the number of aromatic rings)					
1	35.0	50.3	60.3	51.8	72.3
2	59.0	46.3	38.1	32.4	24.1
3	4.7	2.3	0.7	14.8	3.3
4	0.6	0.5	0.4	0.8	0.2

^a 5g of PS and 25g of MgO, separately.

^b Mixture of 5g of PS and 25g of MgO.

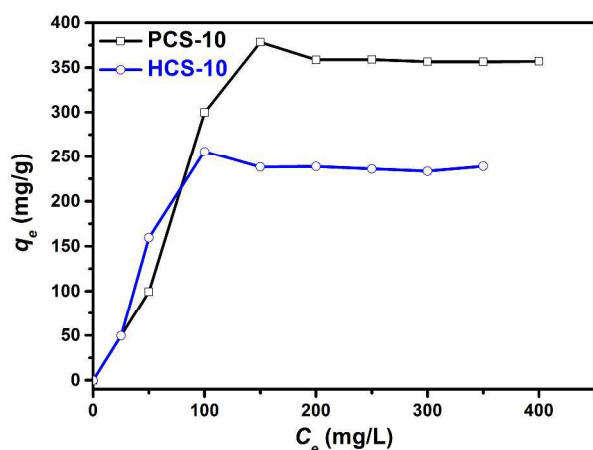


Fig. 11 Equilibrium adsorption isotherms of MB on the PCS-10 and HCS-10.

Fig. 11 displays the equilibrium adsorption isotherms of MB on the PCS-10 and HCS-10. The isotherms were characteristic of the Langmuir isotherm, which was belonged to type I curve. The amount of adsorbed MB increased at a lower final solution concentration, which suggests a high affinity between MB molecules and the surface of PCS and HCS. The adsorbed amount then reached a plateau at a higher equilibrium solution concentration, reflecting the saturated adsorption. The q_m of the PCS-10 for MB was as high as 358.8 mg/g, which was larger than that of HCS-10 (238.6 mg/g). Compared to other adsorbents (Table 4) including CNS,⁸ CNTs,³² graphene oxide,³³ graphene nanosheet,³⁴ activated CS-CNT,² magnetic Ni/C nonmaterial,³⁵ BN hollow sphere,³⁶ montmorillonite,³⁷ alkali-activated CNTs,³⁸ and activated carbon,³⁹ PCS and HCS showed an excellent adsorption performance of MB without any activation. We

believe that both PCS and HCS are the promising materials for many applications to environment management.

Table 4 Comparison of the adsorption capacity of MB using various adsorbents.

Adsorbent	Maximum adsorption capacity (mg/g)	Reference
CNS	30.3	8
CNTs	35.4–64.7	32
Graphene oxide	64.23	33
Graphene nanosheet	111.62	34
Activated CS-CNT	172.4	2
Magnetic Ni/C nanomaterials	165.5–175.2	35
BN hollow sphere	191.7	36
Hollow carbon shell (HCS)	238.6	Present work
Montmorillonite	300.3	37
Porous Carbon sheet (PCS)	358.8	Present work
Alkali-activated CNTs	400.0	38
Activated carbon	452.2	39

Conclusions

We reported a simple approach to prepare porous sheet carbon and hollow carbon shell by catalytic carbonization of PS using MgO as a template and degradation catalyst at 700°C. Porous carbon sheet and hollow carbon shell were prepared by the catalysis of MgO with different morphologies. The yields of porous carbon sheet and hollow carbon shell increased as the

weight ratio of MgO to PS increased. Aromatics with benzene rings more than 3 were the main carbon sources for the growth of nanocarbon. MgO promoted the degradation of PS and acted as a template for the shape-controlled growth of carbon nanostmaterials. MgO can be easily removed by dilute hydrochloric acid to isolate the nanocarbon. The surface area of porous carbon sheet and hollow carbon shell reached 854 and 523 m²/g without any activation, respectively. Porous carbon sheet prepared at a MgO/PS weight ratio of 10 exhibited a adsorption capacity of 358.8 mg/g towards MB from wastewater. The yield of styrene in the liquid products reached 50% by the catalysis of polygonal MgO. This simple strategy provides a removable bifunctional catalyst for degradation of polymer and preparing high-value nanocarbon and useful chemicals.

Acknowledgments

The work was financially supported by the National Natural Science Foundation of China (NSFC 51373171 and 21201155). The work is cofounded by the Natural Science Young Scholars Foundation of Shanxi Province (No: 2012021007-5 and 2013021008-6) and Program for the Top Young Academic Leaders of Higher Learning Institutions of Shanxi and the Innovative Talents of Higher Learning Institutions of Shanxi.

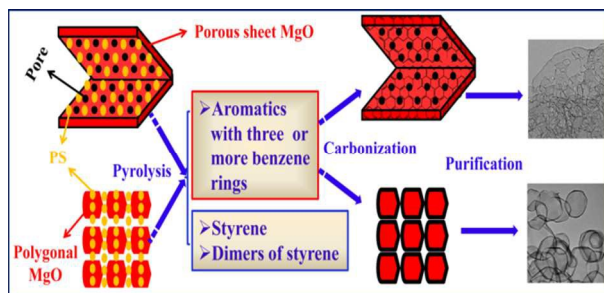
Notes and references

^a Department of Chemistry, College of Science, North University of China, Taiyuan 030051, China

^b State Key Laboratory of Polymer Physics and Chemistry, Changchun Institute of Applied Chemistry, Chinese Academy of Sciences, Changchun 130022, China

† Electronic Supplementary Information (ESI) available: [Yields of the different fractions for the pyrolysis of PS/sheet MgO at different temperatures (Table S1), TEM images and Raman spectra of nanocarbon obtained on sheet MgO (Fig. S1 and Fig. S2), The assignment and area percentage of the compounds in Fig. 10 (Table S2)]. See DOI: 10.1039/b000000x/

- C. Zhuo, B. Hall, H. Richter and Y. Levendis, *Carbon*, 2010, **48**, 4024.
- J. Gong, J. Feng, J. Liu, Z. Jiang, X. Chen, E. Mijowska, X. Wen and T. Tang, *Chem. Eng. J.*, 2014, **248**, 27.
- J. Gong, J. Liu, X. Chen, X. Wen, Z. Jiang, E. Mijowska, Y. Wang and T. Tang, *Micropor. Mesopor. Mat.*, 2013, **176**, 31.
- J. Gong, K. Yao, J. Liu, Z. Jiang, X. Chen, X. Wen, E. Mijowska, N. Tian and T. Tang, *J Mater. Chem. A*, 2013, **1**, 5247.
- L. Wei, N. Yan and Q. Chen, *Environ. Sci. Technol.*, 2011, **45**, 534.
- C. Wu, M. A. Nahil, N. Miskolczi, J. Huang and P. T. Williams, *Environ. Sci. Technol.*, 2014, **48**, 819.
- V. G. Pol, *Environ. Sci. Technol.*, 2010, **44**, 4753.
- J. Gong, J. Liu, X. Chen, Z. Jiang, X. Wen, E. Mijowska and T. Tang, *J Mater. Chem. A*, 2015, **3**, 341.
- J. Gong, J. Liu, L. Ma, X. Wen, X. Chen, D. Wan, H. Yu, Z. Jiang, E. Borowiak-Palen and T. Tang, *Appl. Catal. B: Environ.*, 2012, **117–118**, 185.
- A. Bazargan and G. McKay, *Chem. Eng. J.*, 2012, **195–196**, 377.
- C. Zhuo and Y. A. Levendis, *J. Appl. Polym. Sci.*, 2014, **131**, n/a.
- J. Zhang, B. Yan, S. Wan and Q. Kong, *Ind. Eng. Chem. Res.*, 2013, **52**, 5708.
- V. G. Pol and M. M. Thackeray, *Energ. Environ. Sci.*, 2011, **4**, 1904.
- T. Tang, X. Chen, X. Meng, H. Chen and Y. Ding, *Angew. Chem. Int. Ed.*, 2005, **44**, 1517.
- R. Song, Z. Jiang, W. Bi, W. Cheng, J. Lu, B. Huang and T. Tang, *Chem – Eur. J.*, 2007, **13**, 3234.
- J. Gong, J. Liu, X. Wen, Z. Jiang, X. Chen, E. Mijowska and T. Tang, *Ind. Eng. Chem. Res.*, 2014, **53**, 4173.
- L.-L. Tan, W.-J. Ong, S.-P. Chai and A. R. Mohamed, *Catal. Today*, 2013, **217**, 1.
- H. Wang, X. Sun, Z. Liu and Z. Lei, *Nanoscale*, 2014, **6**, 6577.
- A. Bachmatiuk, R. G. Mendes, C. Hirsch, C. Jähne, M. R. Lohe, J. Grothe, S. Kaskel, L. Fu, R. Klingeler, J. Eckert, P. Wick and M. H. Rummeli, *ACS Nano*, 2013, **7**, 10552.
- J. Zhao, G. Zhu, W. Huang, Z. He, X. Feng, Y. Ma, X. Dong, Q. Fan, L. Wang, Z. Hu, Y. Lu and W. Huang, *J. Mater. Chem.*, 2012, **22**, 19679.
- A. M. Rao, E. Richter, S. Bandow, B. Chase, P. C. Eklund, K. A. Williams, S. Fang, K. R. Subbaswamy, M. Menon, A. Thess, R. E. Smalley, G. Dresselhaus and M. S. Dresselhaus, *Science*, 1997, **275**, 187.
- Z.-H. Sheng, L. Shao, J.-J. Chen, W.-J. Bao, F.-B. Wang and X.-H. Xia, *ACS Nano*, 2011, **5**, 4350.
- Z.-S. Wu, W. Ren, L. Gao, B. Liu, C. Jiang and H.-M. Cheng, *Carbon*, 2009, **47**, 493.
- R. Demir-Cakan, N. Baccile, M. Antonietti and M.-M. Titirici, *Chem. Mater.*, 2009, **21**, 484.
- X. Song, Y. Wang, K. Wang and R. Xu, *Ind. Eng. Chem. Res.*, 2012, **51**, 13438.
- Z. Zhang and J. Kong, *J. Hazard. Mater.*, 2011, **193**, 325.
- H. Hu, X. Wang, J. Wang, F. Liu, M. Zhang and C. Xu, *Appl. Surf. Sci.*, 2011, **257**, 2637.
- N. Li, Z. Wang, K. Zhao, Z. Shi, Z. Gu and S. Xu, *Carbon*, 2010, **48**, 255.
- H. Zhou, C. Wu, J. A. Onwudili, A. Meng, Y. Zhang and P. T. Williams, *Waste Management*, 2015, **36**, 136.
- X. Wan, K. Chen, D. Liu, J. Chen, Q. Miao and J. Xu, *Chem. Mater.*, 2012, **24**, 3906.
- P. T. A. Reilly and W. B. Whitten, *Carbon*, 2006, **44**, 1653.
- Y. Yao, F. Xu, M. Chen, Z. Xu and Z. Zhu, *Bioresour. Technol.*, 2010, **101**, 3040.
- J.-H. Deng, X.-R. Zhang, G.-M. Zeng, J.-L. Gong, Q.-Y. Niu and J. Liang, *Chem. Eng. J.*, 2013, **226**, 189.
- Z.-J. Fan, W. Kai, J. Yan, T. Wei, L.-J. Zhi, J. Feng, Y.-m. Ren, L.-P. Song and F. Wei, *ACS Nano*, 2011, **5**, 191.
- J. Gong, K. Yao, J. Liu, X. Wen, X. Chen, Z. Jiang, E. Mijowska and T. Tang, *Chem. Eng. J.*, 2013, **215–216**, 339.
- G. Lian, X. Zhang, S. Zhang, D. Liu, D. Cui and Q. Wang, *Energ. Environ. Sci.*, 2012, **5**, 7072.
- C. A. P. Almeida, N. A. Debacher, A. J. Downs, L. Cottet and C. A. D. Mello, *J. Colloid Interface Sci.*, 2009, **332**, 46.
- A. H. El-Sheikh, J. A. Sweileh and Y. S. Al-Degs, *Anal. Chim. Acta*, 2007, **604**, 119.
- B. H. Hameed, A. T. M. Din and A. L. Ahmad, *J. Hazard. Mater.*, 2007, **141**, 819.

For Table of Contents only**Conversion of Polystyrene into Porous Carbon Sheet and Hollow Carbon Shell over Different Magnesium Oxide Templates for Efficient Removal of Methylene Blue**Yanliang Wen^{a,b}, Jie Liu,^b Jiangfeng Song,^{*a} Jiang Gong,^b Hao Chen^b and Tao Tang^{*b}

A facile and sustainable approach was established to convert polystyrene into porous carbon sheet and hollow carbon shell over magnesium oxide templates with different morphologies.